Journal of Alloys and Compounds 506 (2010) 4–9

Contents lists available at ScienceDirect

Journal of Alloys and Compounds

journal homepage: www.elsevier.com/locate/jallcom

Spectroscopic and crystal field studies of $LiAlO_2$:Mn^{2+} single crystals

M.G. Brik[a,*], Hao Teng[b], Hui Lin[b], Shengming Zhou[b], N.M. Avram[c,d]

[a] Institute of Physics, University of Tartu, Riia 142, Tartu 51014, Estonia
[b] Key Laboratory of Material Science and Technology for High Power Lasers, Shanghai Institute of Optics and Fine Mechanics, Chinese Academy of Sciences, Jiading District, Shanghai 201800, China
[c] Department of Physics, West University of Timisoara, Bd. V. Parvan 4, Timisoara 300223, Romania
[d] Academy of Romanian Scientists, Independentei 54, Bucharest 050094, Romania

ARTICLE INFO

Article history:
Received 25 May 2010
Received in revised form 18 June 2010
Accepted 23 June 2010

Keywords:
Crystal field
Mn^{2+}
Absorption spectra

ABSTRACT

$LiAlO_2$:Mn^{2+} high-quality single crystals were grown by Czochralski technique. Room-temperature excitation and emission spectra were recorded in the spectral range from 220 to 750 nm. For the first time, detailed crystal field analysis (based on the exchange charge model of crystal field) has been performed for Mn^{2+} ions in this host. Calculated crystal field parameters were used for diagonalization of the crystal field Hamiltonian in the basis set consisting from all wave functions of the LS terms of Mn^{2+} ions. Calculated positions and splittings of the Mn^{2+} energy levels are in good agreement with main peaks in the experimental excitation and emission spectra and widths of the observed spectral bands. It was established from the symmetry analysis of the Li^+ and Al^{3+} positions that the former can be described by the C_2 point group, whereas the latter by the D_2 point group.

1. Introduction

Transition metal ions with an unfilled 3d electron shell are being successfully used for a long time as active ions for getting tunable laser generation or luminescence in a wide spectral region: from infrared to visible parts of the spectrum [1–4]. A large variety of different combinations "host crystal + impurity ion" have been studied so far. In the present work we focus our attention on the Mn^{2+}-doped $LiAlO_2$ (γ-phase) single crystals. Mn^{2+} ions exhibit luminescence in a visible spectral region (at about 570 nm), and are used in various phosphor materials [5–8]. Since excited energy levels of Mn^{2+} match some of the trivalent lanthanides energy levels, Mn^{2+} ions are also used for co-doping and efficient energy transfer between co-dopants [9–11]. As for the $LiAlO_2$, recently it attracted interest of researchers due to its application for growing GaN layers [12]. Several research works have been published, which were focused upon experimental spectroscopic studies of $LiAlO_2$ crystals doped with Cr^{4+} [13,14], V^{3+} [15,16], Fe^{3+} [17], Mn^{2+} [18,19]. In those studies, it was emphasized that only tetrahedral sites are available for doping in $LiAlO_2$, which makes this crystal to be an ideal host for studies of spectroscopic properties of transition metal ions in the fourfold coordination. It should be mentioned, however, that the crystal growth of high-quality $LiAlO_2$ single crystals is related to a number of difficulties.

Recently [19], successful crystal growth of high-quality $LiAlO_2$:Mn^{2+} single crystals has been reported. In the present paper we extend those previous studies by adding detailed crystal field analysis of Mn^{2+} energy levels and comparison with experimental excitation and emission spectra. In the next sections we describe separately experimental and theoretical parts of the present study, discuss the obtained results, analyze the symmetry properties of the cation's sites in γ-$LiAlO_2$ and conclude the paper with a short summary.

2. Samples preparation, crystal structure and spectroscopic measurements

The $LiAlO_2$:Mn^{2+} single crystals studied in the present work were grown by the radio frequency heating Czochralski pulling method from initial mixture of Li_2CO_3, Al_2O_3 and MnO_2. All the details of crystal growth are described in Ref. [19] and are not repeated here for the sake of brevity. The as-grown crystals were about 10 cm in length, transparent and almost colorless. The (1 0 0) wafers were cut from the boule and chemo-mechanically polished. The thickness of all polished wafers was 1 mm. X-ray diffraction studies confirmed crystal structure of γ-$LiAlO_2$. The Mn concentration was 0.034 at% at the growth starting position and 0.3 at% in the melt. Excitation and emission spectra were measured employing a FP-6500/6600 fluorescence spectrometer (JASCO Inc., Japan) in the spectral range from 220 to 750 nm.

The γ-phase of $LiAlO_2$ crystallizes in the $P4_12_12$ space group with the lattice constants (all in Å): $a = b = 5.1687(5)$; $c = 6.2679(6)$

* Corresponding author.
E-mail address: brik@fi.tartu.ee (M.G. Brik).

0925-8388/$ – see front matter © 2010 Elsevier B.V. All rights reserved.
doi:10.1016/j.jallcom.2010.06.160

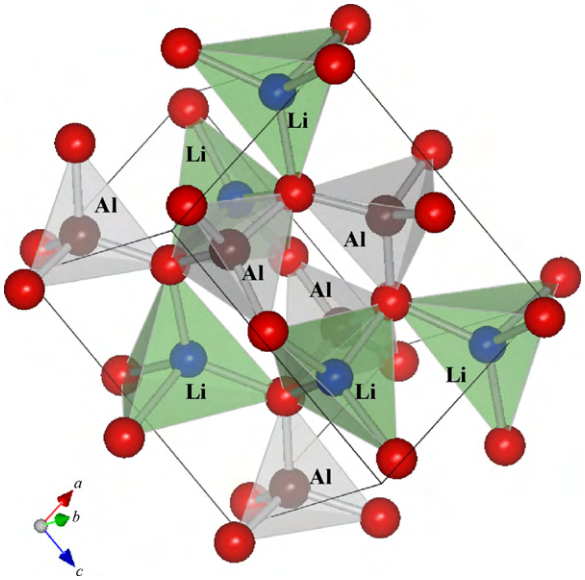

Fig. 1. One unit cell of γ-$LiAlO_2$ crystal. Alternating coordination polyhedra around Al and Li ions made by four oxygen ions each are shown. Drawn with VENUS developed by Izumi and Dilanian. Orientation of the crystallographic axes *a*, *b*, and *c* is shown.

[20]. One unit cell contains 4 formula units. Each Al ion is surrounded by four oxygen ions, with the Al–O distances 1.7553 Å (two bonds) and 1.7663 Å (two bonds). Each Li ion is also fourfold coordinated by oxygen ions, with distances 1.9480 and 2.0595 Å (each bond is repeated twice). Fig. 1 depicts one unit cell of $LiAlO_2$ crystal; fourfold coordination around Li and Al ions is shown.

From the point of view of ionic radii ($r(Li^+) = 0.068$ nm, $r(Al^{3+}) = 0.057$ nm [21], $r(Mn^{2+}) = 0.08$ nm [22]), it looks more likely that after doping, Mn^{2+} ions substitute for Li^+ ions. An excessive positive charge, which is introduced into a crystal after doping, can be compensated by creation of the Li^+ vacancies, randomly distributed in the volume of the samples.

Fig. 2 shows transmittance spectrum of $LiAlO_2$:Mn^{2+} crystal in the spectral range from 190 to 1500 nm. The sample is transparent in the whole studied spectral range (transmittance is more than 85%). Absorption edge is about 200 nm, which allows for estimations of the band gap to be about 6.2 eV. As seen from Fig. 2, no special bands ascribing to the Mn ions were detected. They have a very low intensity, since they are parity- and spin-forbidden, which determines the colorless appearance of the as-grown crystals.

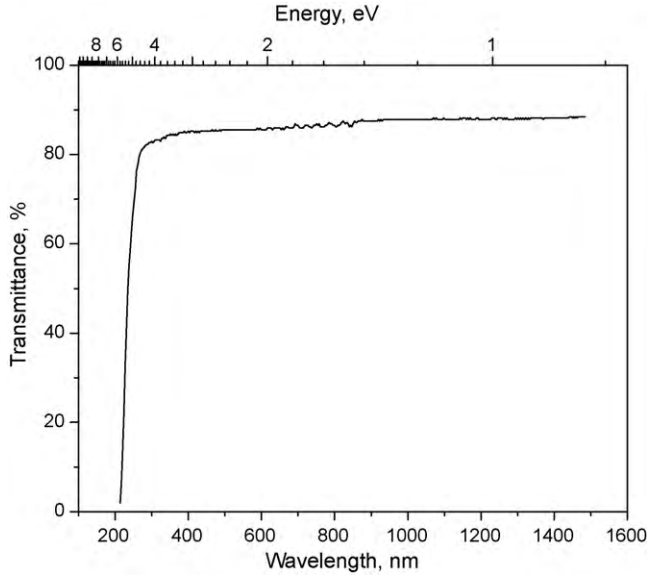

Fig. 2. Transmittance spectrum of $LiAlO_2$:Mn^{2+}.

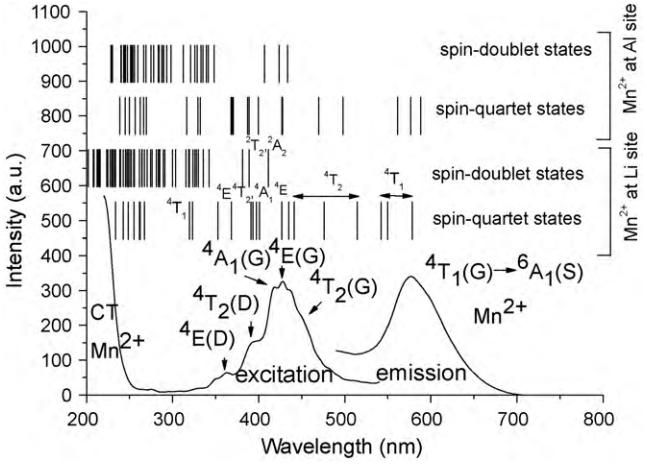

Fig. 3. Comparison between the calculated energy levels of Mn^{2+} (vertical lines, from top to bottom: spin-doublet states of Mn ions at Al position, spin-quartet states of Mn ions at Al position, spin-doublet states of Mn ions at Li position, spin-quartet states of Mn ions at Li position, respectively) and the experimental excitation and emission spectra of $LiAlO_2$:Mn^{2+}. Assignment of the calculated levels is shown only for Li site and is the same for Al site.

The room-temperature experimental excitation and emission spectra are shown in Fig. 3. The emission spectrum is determined by a wide $^4T_1(^4G) \rightarrow {}^6A_1(^6S)$ band centered at 577 nm. The most prominent absorption peak is due to the $^6A_1(^6S) \rightarrow {}^4E(^4G)$ absorption transition at 428 nm, with a shoulder at about 450 nm ($^6A_1(^6S) \rightarrow {}^4T_2(^4G)$ transition) and a peak at 417 nm ($^6A_1(^6S) \rightarrow {}^4A_1(^4G)$ transition). Two additional peaks at about 390 and 360 nm are due to the transitions to the $^4T_2(^4D)$ and $^4E(^4D)$ states, respectively. A very intensive band to the left from 250 nm is caused by the O^{2-}–Mn^{2+} charge transfer transition [23].

3. Method of calculations

It is a standard practice in the theory of crystal field, to calculate the energy levels of an impurity ion with an unfilled d-shell as the eigenvalues of the following crystal field Hamiltonian:

$$H = \sum_{p=2,4} \sum_{k=-p}^{p} B_p^k O_p^k. \quad (1)$$

In this equation O_p^k operators are the suitably chosen linear combinations of the irreducible tensor operators, which act on the angular parts of the impurity ion's wave functions. At this point it should be mentioned that various definitions of these operators have been used in the literature so far (an interested reader may wish to look for further details into Refs. [24,25]). In this paper we shall consistently follow Ref. [26] in definition of the O_p^k operators, which corresponds to the Stevens normalization. All necessary equations can be found in Ref. [26] and thus are not reproduced here. The B_p^k entries are the so-called crystal field parameters (CFPs), which can be calculated directly from the crystal structure data. The number of non-zero CFPs for 3d ions depends on the local site symmetry and can vary from just 1 in the case of perfect cubic symmetry to 14, when the local symmetry is described by the C_1 point group.

In the exchange charge model (ECM) of crystal field, the CFPs B_p^k are represented as a sum of two different contributions [26]:

$$B_p^k = B_{p,q}^k + B_{p,S}^k, \quad (2)$$

where

$$B^k_{p,q} = -K^k_p e^2 \langle r^p \rangle \sum_i q_i \frac{V^k_p(\theta_i, \varphi_i)}{R_i{}^{p+1}}, \quad (3)$$

$$B^k_{p,S} = K^k_p e^2 \frac{2(2p+1)}{5} \sum_i (G_s S(s)_i{}^2 + G_\sigma S(\sigma)_i{}^2 + \gamma_p G_\pi S(\pi)_i{}^2) \frac{V^k_p(\theta_i, \varphi_i)}{R_i}. \quad (4)$$

The first term $B^k_{p,q}$ is the point charge contribution to the CFPs, which is due to the electrostatic interaction between the central ion and the crystal lattice ions enumerated by index i with charges q_i and spherical coordinates, R_i, θ_i, φ_i (with the reference system centered at the impurity ion itself). The averaged values $\langle r^p \rangle$, with r being the radial coordinate of the d electrons of the impurity ion, can be obtained either from the literature or calculated numerically, using the radial parts of the corresponding ion's wave functions. The values of the numerical factors K^k_p, γ_p, the expressions for the polynomials V^k_p and the definitions of the operators O^k_p can all be found in Ref. [26]. In Eq. (3) the crystal lattice ions are treated as the point charges only, and their specific quantum mechanical properties are not accounted for. It is the second term $B^k_{p,S}$ given by Eq. (4) that enormously improves the old point charge model of crystal field. $B^k_{p,S}$ is proportional to the overlap between the wave functions of the central ion and ligands (different s-, p-, and d-states), thus distinguishing between different quantum mechanical states of interacting ions and including into consideration all covalent effects. $S(s)$, $S(\sigma)$, $S(\pi)$ in Eq. (4) correspond to the overlap integrals between the d-functions of the central ion and p-, s-functions of ligands: $S(s) = \langle d0|s0\rangle$, $S(\sigma) = \langle d0|p0\rangle$, $S(\pi) = \langle d1|p1\rangle$ (here the $\langle lm|$ notation is employed, where l and m are the orbital and magnetic quantum numbers, respectively). The G_s, G_σ, G_π entries are the dimensionless adjustable parameters of the model, whose values are determined from the positions of the first three absorption bands in the experimental spectrum by a direct matching calculated energy levels to those deduced from the experimental spectra. They can be approximated to a single value, i.e. $G_s = G_\sigma = G_\pi = G$, which then can be estimated from one absorption band only. This is usually a reasonable approximation [26] and constitutes one of the main advantages of ECM, namely, remarkable ability to give a reasonable description of the experimental spectroscopic data with a single fitting parameter only.

Until now, the ECM has been shown to be a reliable tool for successful description of spectra of rare earth ions [26–28] and transition metal ions [29–33], which serves as a firm justification of application of ECM for $LiAlO_2$:Mn^{2+}.

4. Crystal field calculations of Mn^{2+} energy levels in $LiAlO_2$

Mn^{2+} ions have the $3d^5$ electron configuration, which corresponds to exactly half-filled d-shell. The Coulomb interaction among these five electrons gives rise to 16 LS terms: one spin-sextet ^{6}S, four spin-quartets ^{4}PDFG, and eleven spin-doublets ^{2}SPD$_{(3)}$F$_{(2)}$G$_{(2)}$HI (the subscript in the parenthesis indicates the number of repeating terms with the same values of L and S). The ground state is the ^{6}S term, which in the tetrahedral crystal field is not split and transforms according to the A_1 irreducible representation. As it is easy to see, for Mn^{2+} all absorption and emission transitions from/to the ground state are essentially spin-forbidden.

To apply the ECM equations (3) and (4), the structural data from Ref. [20] were used to generate a large cluster consisting of 44,296 ions with a Li^+ ion (replaced by a Mn^{2+}) ion at the center. No assumptions on the symmetry of the Mn^{2+} position were made.

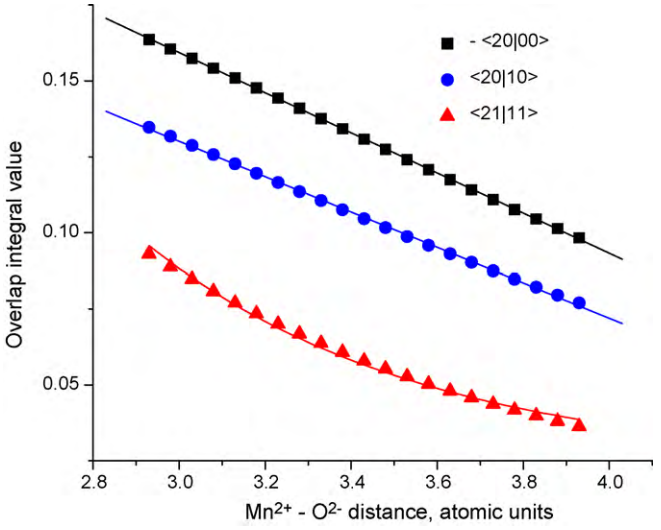

Fig. 4. Calculated values of the overlap integrals (⟨20|00⟩ – squares, ⟨20|10⟩ – circles, and ⟨21|11⟩ – triangles) and their approximating functions (Eqs. (5), (6) and (7), correspondingly). Note that the sign of the ⟨20|00⟩ calculated values is changed in the figure, in order to show all overlap integrals in a closer region for better illustration of their distance dependence.

The overlap integrals between the Mn^{2+} and the O^{2-} wave functions for various interionic distances were calculated numerically using the radial parts of the wave functions from Refs. [34,35]. Fig. 4 shows the calculated values (by symbols); for the convenience of further use they were approximated by the following functions of the interionic distance R (measured in atomic units):

$$S_s = \langle d0|s0\rangle = -0.3229 + 0.063363R, \quad (5)$$

$$S_\sigma = \langle d0|p0\rangle = 0.27169 - 0.054574R, \quad (6)$$

$$S_\pi = \langle d1|p1\rangle = 1.4757 \exp(-0.94354R). \quad (7)$$

These approximating lines are also shown in Fig. 4.

Although it is more probable that Mn^{2+} ions substitute for Li^+ ions, another opportunity – when Mn ion enter $LiAlO_2$ lattice at Al^{3+} position, may not be completely eliminated. For the sake of completeness of our study, we have also performed the calculations of the divalent manganese energy levels assuming this opportunity.

Table 1 shows the calculated values of the CFPs (which were obtained using Eqs. (1)–(7)) for both considered positions of impurity. The values of the ECM fitting parameter G was obtained from the experimentally detected position of the first excited state $^4T_1$ of Mn^{2+} ion and turned out to be 3.17 for the Li site and 1.2 for the Al site. Both contributions to the total CFPs are shown separately in Table 1. It is seen that the $B^k_{p,S}$ parameters are greater than the $B^k_{p,q}$ parameters, which shows importance of the overlap and exchange interactions for a proper analysis of the crystal field effects in the $LiAlO_2$:Mn^{2+} system.

The crystal field Hamiltonian (1) with the CFPs from Table 1 was diagonalized in the space spanned by 100 wave functions of all LS terms of the d^5 electron configuration of Mn^{2+}. The spin–orbit interaction was not included, since no fine structure of the absorption band was detected. The Racah parameters B and C were estimated from the barycenters of the energy levels arising from the ^{4}G term (four states: $^4T_1$, $^4T_2$, ^4E, $^4A_1$) and ^{4}D term (two states: ^4E, $^4T_2$). They turned out to be (in cm^{-1}) $B = 702$ and $C = 2941$; the Trees' correction constant $\alpha = 85\ cm^{-1}$ is within the typical range of this constant for Mn^{2+} reported in the literature (from 76 cm^{-1} [36] to 181 cm^{-1} [37]). The calculated energy levels are shown in Fig. 3 by vertical lines, which are superimposed onto the experimental excitation and emission spectra. As seen from this figure, agree-

Table 1
The CFPs values (all in cm^{-1}; Stevens normalization) for Mn^{2+} ions at Li and Al sites in $LiAlO_2$.

	Li site			Al site		
	$B^k_{p,q}$	$B^k_{p,S}$	Total value	$B^k_{p,q}$	$B^k_{p,S}$	Total value
B^{-2}_2	1693.7	2561.5	4255.2	2202.9	788.4	2991.3
B^{-1}_2	2272.5	1116.0	3388.5	2168.8	327.2	2496.0
B^0_2	2547.7	1833.4	4381.1	496.3	67.7	564.0
B^1_2	−2272.5	−1116.0	−3388.5	−2168.8	−327.2	−2496.0
B^2_2	0.0	0.0	0.0	0.0	0.0	0.0
B^{-4}_4	0.0	0.0	0.0	0.0	0.0	0.0
B^{-3}_4	401.6	−540.5	−138.9	−873.0	−1108.3	−1981.3
B^{-2}_4	2075.2	3786.3	5861.5	4917.6	3685.6	8603.2
B^{-1}_4	784.2	1677.0	2461.2	1487.0	1177.5	2664.5
B^0_4	239.5	558.7	798.2	258.2	165.7	423.9
B^1_4	−784.2	−1677.0	−2461.2	−1487.0	−1144.5	−2664.5
B^2_4	0.0	0.0	0.0	0.0	0.0	0.0
B^3_4	401.6	−540.5	−138.9	−873.0	−1108.3	−1981.3
B^4_4	3028.0	4732.5	7760.5	5025.5	3835.9	8861.4

ment between the calculated Mn^{2+} energy levels and main peaks and their features is good. Being based on the crystal field calculations, it is difficult to say which position can be occupied with a greater probability. The ab initio calculations can help in answering this question, but it is beyond the scope of the present study. However, we believe that the Mn^{2+} ions mainly occupy the Li positions in $LiAlO_2$. Splitting of the Mn^{2+} orbital triplet states for the Al site is somewhat smaller than for the Li^+ site, which indicates a higher symmetry of the former position. It is also easy to see that the density of the Mn^{2+} calculated states in the spectral range from 400 to 200 nm is quite high. These states are the spin-quartets and spin-doublets (mainly), all of which are hidden behind a very intensive charge transfer band, which starts at about 250 nm.

The calculated energy levels of Mn^{2+} in comparison with the experimentally deduced energy levels are shown in Table 2. Since the symmetry of the Mn^{2+} position is low, all orbital triplet and doublet states are split into orbital singlets, which can explain broad absorption and emission bands. For example, the calculated splitting of the $^4T_1(^4G)$ state is about 1200 cm^{-1}, and the experimental full width at half maximum (FWHM) is about 2000 cm^{-1}. The calculated splitting of the $^4E(^4D)$ state is about 1600 cm^{-1}, which correlates with the widths of the $^4E(^4D)$ absorption feature in Fig. 2 (about 1500 cm^{-1}). We also note here that all absorption transitions are broadened by electron–vibrational interaction, which is not taken into account in calculations of the crystal field energy levels. Positions of the spin-doublet states are not indicated in Table 2, because the absorption transitions to the spin-doublet states from the $^6A_1$ state are much weaker than absorption transitions to the spin-quartet states, and, therefore, they cannot be seen in the experimental spectra.

Inspection of Table 2 together with Fig. 2 shows good agreement between the calculated Mn^{2+} energy levels and the experimental spectra.

It should be mentioned that the $^6A_1$–$^4T_1$ transition is forbidden by the group selection rules, whereas the $^6A_1$–$^4T_2$ is allowed. Due to this circumstance (in combination with low-symmetry splitting of the orbital triplets), precise experimental determination of the $^4T_1$ level position from the absorption spectrum is rather ambiguous. It was found earlier that in fluorite lattices the Stokes shift between the Mn^{2+} emission and the absorption is about 1500 cm^{-1} [38], so from this point of view the two highest calculated levels – 18197 and 18439 cm^{-1} (Table 2) – are more reliable estimations of the $^4T_1(^4G)$ level position.

Using the Tanabe–Sugano matrices [39] and barycenters of the calculated energy levels from Table 2 along with the above-given values of the Racah parameters, it is possible to estimate the 10*Dq* parameter for $LiAlO_2$:Mn^{2+} to be about 760 cm^{-1}. Such a value agrees with recently reported values for Mn^{2+} in tetrahedral positions in $MgGa_2O_4$ (784–798 cm^{-1} [37]). As it can be anticipated, 10*Dq* for Mn^{2+} in a tetrahedral complex is smaller than in an octahedral complex (933–968 cm^{-1} [37]).

Calculated positions of the spin-doublets and highly located spin-quartets are not included in Table 2, since they do not have any immediate relation to the experimental spectra shown in Fig. 3.

We also note here that usually, when Mn^{2+} energy levels are analyzed, a cubic crystal field approximation is invoked based on the Tanabe–Sugano theory [39], which does not allow at all to treat the low-symmetry splittings of orbitally degenerated levels, calculated in the present work. Table 3 shows comparison between the previously reported in the literature values of the Racah parameters *B*, *C* and Trees' correction α with those for $LiAlO_2$:Mn^{2+}. Data

Table 2
Comparison between the calculated and the observed energy levels of Mn^{2+} in $LiAlO_2$. Only spin-quartet energy levels from the experimentally studied spectral range are shown.

Energy (cm^{-1})			"Parent" T_d group irreducible representations
Calculated		Observed	
Al site	Li site		
0	0	0	$^6A_1$
17,000, 17,337, 17,816	17,291, 18,197, 18,439	17,330 (577 nm)	$^4T_1(^4G)$
20,091, 21,287, 21,791	19,430, 20,998, 22,661	22,026 (454 nm)	$^4T_2(^4G)$
23,372, 23,416, 23,425	23,000, 23,417, 23,428	23,364 (428 nm) 23,981(417 nm)	^4E, $^4A_1(^4G)$
25,043, 25,738, 25,827	24,945, 25,177, 25,422	25,641 (390 nm)	$^4T_2(^4G)$
26,988, 27,102	25,559, 27,147	27,728 (360 nm)	$^4E(^4D)$
30,131, 30,387, 31,639	28,369, 30,943, 31,299	29,412 (340 nm)	$^4T_1(^4P)$

Table 3
Racah parameters B, C and Trees' correction α (all in cm^{-1}) for Mn^{2+} ions in different crystals.

Parameter	$LiAlO_2$ (this work)	$MgGa_2O_4$ [37]	$C_4H_{12}N_2O_6$ [40]	$K[CS(NH_2)_2]_4Br$ [41]	$KZnClSO_4{\cdot}3H_2O$ [42]	$Cd(C_4H_2O_4){\cdot}2H_2O$ [43]
B	702	665	752	784	657	844
C	2941	–	2438	2762	3103	3010
α	85	181	76	76	76	–

Table 4
Coordinates (in Å) of ions in the $[MnO_4]^{6-}$ cluster. The X, Y, Z axes coincide with the crystallographic axes a, b, c.

Ions	X	Y	Z	Distance
Mn^{2+}	0	0	0	0
O_1^{2-}	−0.7727	−0.5334	1.7068	1.9480
O_2^{2-}	2.0509	0.1256	0.1398	2.0595
O_3^{2-}	−0.5334	−0.7727	−1.7068	1.9480
O_4^{2-}	0.1256	2.0509	−0.1398	2.0595

collected in Table 3 confirm validity of the B, C, and α parameters used in the present work.

5. Analysis of symmetry properties of Li and Al positions in $LiAlO_2$

At this point – after having performed the energy level calculations without any symmetry approximations – it is instructive to come back to the question of what the actual symmetry of the Mn^{2+} position (at Li^+ site) is. It can be expected to be quite low, since degeneracy of all energy levels is taken off completely. Precise analysis of the symmetry properties of impurity centers in crystals can be effectively performed using the "Symmetry" program developed by Cavalli and Cammi [44,45]. Coordinates of the four nearest oxygen ions around a lithium ion are given in Table 4.

The angles between the oxygen ligands are as follows (all in°): O_1^{2-}–O_2^{2-} = 110.6254; O_1^{2-}–O_3^{2-} = 123.3964; O_1^{2-}–O_4^{2-} = 110.8755; O_2^{2-}–O_3^{2-} = 110.8755; O_2^{2-}–O_4^{2-} = 83.2894; O_3^{2-}–O_4^{2-} = 110.6254. Also all angles differ from the perfect tetrahedron angle of 109.45°, the difference is not very large for some of them. The symmetry analysis of the $[MnO_4]^{6-}$ unit shows that the distortion from the "parent" T_d symmetry is given by the following pathway: $T_d \rightarrow D_2$ (50%) $\rightarrow C_{2v}$ (99.99%) $\rightarrow C_2$ (100%). The values in parenthesis indicate the approximation degrees of the distorted geometries. So, D_2 approximation of the local symmetry for the $[MnO_4]^{6-}$ cluster in $LiAlO_2$ will be quite pure, but C_{2v} or C_2 point groups can describe the local symmetry properties quite adequately.

For the sake of completeness, we also consider now the symmetry properties of the Al^{3+} position, which can be occupied by Cr^{4+} or V^{3+} ions [2]. Coordinates of the four nearest oxygen ions around the Al^{3+} ion are shown in Table 5.

The angles between the oxygen ligands are as follows (all in°): O_1^{2-}–O_2^{2-} = 110.6670; O_1^{2-}–O_3^{2-} = 109.9311; O_1^{2-}–O_4^{2-} = 111.8923; O_2^{2-}–O_3^{2-} = 111.8923; O_2^{2-}–O_4^{2-} = 101.5817; O_3^{2-}–O_4^{2-} = 110.6670. All these values are considerably closer to the ideal tetrahedron angle, suggesting somewhat higher symmetry of the Al^{3+} position than that one of the Li^+ site. The distortion from the "parent" T_d symmetry for the Al^{3+} site is given by the following pathway: $T_d \rightarrow D_2$ (79%) $\rightarrow C_{2v}$ (98.9%) $\rightarrow C_2$ (100%). The values in parenthesis indicate the approximation degrees of the distorted geometries. So, already the D_2 approximation of the local symmetry for the $[AlO_4]^{5-}$ cluster in $LiAlO_2$ can be quite reasonable as a first approximation.

Table 5
Coordinates (in Å) of ions in the $[AlO_4]^{5-}$ cluster. The X, Y, Z axes coincide with the crystallographic axes a, b, c.

Ions	X	Y	Z	Distance
Al^{3+}	0	0	0	0
O_1^{2-}	0.8322	0.5928	−1.4272	1.7553
O_2^{2-}	0.1732	−1.7522	0.1398	1.7663
O_3^{2-}	0.5928	0.8322	1.4272	1.7553
O_4^{2-}	−1.7522	0.1732	−0.1398	1.7663

6. Conclusions

In the present paper we report on preparation (Czochralski method), spectroscopic and crystal field studies of high-quality $LiAlO_2$:Mn^{2+} single crystals. Experimental excitation and emission spectra were recorded at room temperature. The exchange charge model of crystal field was applied for calculations of parameters of crystal field acting on the impurity Mn^{2+} ions at the Li^+ sites. As follows from the results of the crystal field calculations, the exchange charge contribution to the crystal field parameters considerably exceeds the point charge contribution, thus showing importance of the covalent and overlap effects on formation of the Mn^{2+} energy levels in $LiAlO_2$. The calculated energy level scheme of Mn^{2+} agrees favorably with experimental excitation and emission spectra of $LiAlO_2$:Mn^{2+} single crystals. Calculated low-symmetry splittings of the orbital triplet and doublet states correlate with overall widths of the observed spectral bands. Estimated from the experimental spectra values of the Racah parameters B and C for Mn^{2+} in $LiAlO_2$ were found to be considerably reduced in comparison with their free ion's counterparts, indicating high degree of covalency of the Mn^{2+}–O^{2-} chemical bonds.

Symmetry analysis of the $[MnO_4]^{6-}$ cluster (Li^+ site) in $LiAlO_2$ was performed and it was established that the C_{2v} or C_2 point groups can be used for describing symmetry properties of impurity center. It was also shown that the Al^{3+} position has somewhat higher symmetry and can be reasonably described with employing the D_2 point group.

References

[1] B. Henderson, R.H. Bartram, Crystal-field Engineering of Solid-State Laser Materials, Cambridge University Press, 2000.
[2] S. Kück, Appl. Phys. B 72 (2001) 515.
[3] A. Sennaroglu, Prog. Quant. Electron. 26 (2002) 287.
[4] Y. Kaliski, Prog. Quant. Electron. 28 (2004) 249.
[5] V. Singh, R.P.S. Chakradhar, J.L. Rao, D.K. Kim, J. Lumin. 128 (2008) 1474.
[6] K.I. Seo, J.H. Park, J.S. Kim, G.C. Kim, J.H. Yoo, J. Lumin. 129 (2009) 715.
[7] X. Yu, Y.H. Wang, J. Phys. Chem. Solids 70 (2009) 1146.
[8] Y.Q. Jiang, J. Chen, Z.X. Xie, L.S. Zheng, Mat. Chem. Phys. 120 (2010) 313.
[9] X.H. Xu, Y.H. Wang, Y.Q. Li, Y. Gong, J. Appl. Phys. 105 (2009) 083502.
[10] P.L. Li, Z.J. Wang, Z.P. Yang, Q.L. Guo, J. Electrochem. Soc. 157 (2010) H504.
[11] C.H. Huang, T.M. Chen, Opt. Express 18 (2010) 5089.
[12] T.H. Huang, S.M. Zhou, H. Teng, H. Lin, J. Wang, Cryst. Res. Tech. 43 (2008) 801.
[13] S. Kück, S. Hartung, K. Petermann, G. Huber, Appl. Phys. B 61 (1995) 33.
[14] S. Kück, S. Hartung, Chem. Phys. 240 (1999) 387.
[15] S. Kück, P. Jander, Chem. Phys. Lett. 300 (1999) 189.
[16] S. Kück, P. Jander, Opt. Mater. 13 (1999) 299.
[17] D.A. Davies, J. Silver, P.J. Titler, R. Haywood, in: M.F. Thomas, J.M. Williams, T.C. Gibb (Eds.), Hyperfine Interactions (C), vol. 5, 2002, p. 341.
[18] B. Dhabekar, E.A. Raja, S. Menon, T.K.G. Rao, R.K. Kher, B.C. Bhatt, Radiat. Meas. 43 (291) (2008).
[19] H. Teng, S.M. Zhou, H. Lin, T.T. Jia, X.R. Hou, J. Wang, Chin. Opt. Lett. 8 (2010) 414.
[20] M. Marezio, Acta Crystallogr. 19 (1965) 396.
[21] T. Depci, G. Özbayoğlu, A. Yilmaz, A.N. Yazici, Nucl. Instr. Meth., Phys. Res. B 266 (2008) 755.
[22] G. Che, C. Liu, Z.X. Li, Z. Xu, Y. Liu, H. Wang, J. Phys. Chem. Solids 69 (2008) 2091.
[23] L. Lin, M. Yin, C. Shi, W. Zhang, J. Alloys Compd. 455 (2008) 327.

[24] C. Rudowicz, J. Phys. C: Solid State Phys. 18 (1985) 1415.
[25] C. Rudowicz, J. Phys. C: Solid State Phys. 18 (1985) 3837.
[26] B.Z. Malkin, in: A.A. Kaplyanskii, B.M. Macfarlane (Eds.), Spectroscopy of Solids Containing Rare-Earth Ions, North-Holland, Amsterdam, 1987, p. 33.
[27] M.N. Popova, E.P. Chukalina, T.N. Stanislavchuk, B.Z. Malkin, A.R. Zaripov, E. Antic-Fidancev, E.A. Popova, L.N. Bezmaternykh, V.L. Temerov, Phys. Rev. B 75 (2007) 224435.
[28] M. Kirm, G. Stryganyuk, S. Vielhauer, G. Zimmerer, V.N. Makhov, B.Z. Malkin, O.V. Solovyev, R.Yu. Abdulsabirov, S.L. Korableva, Phys. Rev. B 75 (2007) 075111.
[29] S.I. Klokishner, B.S. Tsukerblat, O.S. Reu, A.V. Palii, S.M. Ostrovsky, Opt. Mater. 27 (2005) 1445.
[30] C. Jousseaume, D. Vivien, A. Kahn-Harari, B.Z. Malkin, Opt. Mater. 24 (2003) 143.
[31] M.G. Brik, C.N. Avram, N.M. Avram, Spectrochim. Acta A 63 (2006) 759.
[32] M. Vaida, C.N. Avram, Acta Phys. Pol. A 116 (2009) 541.
[33] M.L. Stanciu, M.G. Ciresan, N.M. Avram, Acta Phys. Pol. A 116 (2009) 544.
[34] E. Clementi, C. Roetti, Atom. Data Nucl. Data Tables 14 (1974) 177.
[35] M.V. Eremin, in: A.A. Kaplyanskii (Ed.), Spectroscopy of Laser Crystals, Leningrad, Nauka, 1989, p. 30 (in Russian).
[36] J.L. Rao, B.O.P. Raju, N.O. Gopal, K.V. Narasimhulu, Physica B 355 (2005) 207.
[37] G.K.B. Costa, S.S. Pedro, J.C.S. Carvalho, L.P. Sosman, Opt. Mater. 31 (2009) 1620.
[38] M.T. Barriuso, M. Moreno, J.A. Aramburu, Phys. Rev. B 65 (2002) 064441.
[39] S. Sugano, Y. Tanabe, H. Kamimura, Multiplets of Transition-Metal Ions in Crystals, Acad. Press, New York, 1970.
[40] R. Kripal, H. Govind, M. Bajpai, M. Maurya, Spectrochim. Acta A 71 (2008) 1301.
[41] B. Sudhakar Reddy, N.O. Gopal, K.V. Narasimhulu, Ch. Linga Raju, J.L. Rao, B.C.V. Reddy, J. Mol. Struct. 751 (2005) 161.
[42] J.L. Rao, B.D.P. Raju, N.O. Gopal, K.V. Narasimhulu, Physica B 355 (2005) 207.
[43] X. Yang, X.Y. Kuang, C. Lu, H. Wang, Eur. Phys. J. D 42 (2007) 35.
[44] E. Cavalli, R. Cammi, Acta Cryst. B 48 (1992) 245.
[45] E. Cavalli, R. Cammi, Comput. Chem. 18 (1994) 405.